Research Square

Preprints are preliminary reports that have not undergone peer review.
They should not be considered conclusive, used to inform clinical practice,
or referenced by the media as validated information.

Robust Single-Dose rAAV Dual-Targeting PCSK9/APOC3 via an Optimized Triple-Plasmid System for Ameliorating Mixed Hyperlipidemia

Jia He
Second Affiliated Hospital of Chongqing Medical University
Yunyu He
Chongqing Medical University
Yunfei Zhao
Second Affiliated Hospital of Chongqing Medical University
Gang Zou
Second Affiliated Hospital of Chongqing Medical University
Mengjiao Deng
Second Affiliated Hospital of Chongqing Medical University
Liming Yang
Second Affiliated Hospital of Chongqing Medical University
Ke Hu
Second Affiliated Hospital of Chongqing Medical University
Yaxi Chen
Second Affiliated Hospital of Chongqing Medical University
Chao Yu
yuchao@cqmu.edu.cn

Chongqing Medical University

Research Article

Keywords:

Posted Date: November 18th, 2026

DOI: https://doi.org/10.21203/rs.3.rs-11619935/v1

License: This work is licensed under a Creative Commons Attribution 4.0 International License.
Read Full License

Additional Declarations: No competing interests reported.

Robust Single-Dose rAAV Dual-Targeting PCSK9/APOC3 via an Optimized Triple-Plasmid System for Ameliorating Mixed Hyperlipidemia

Jia He[1#], Yunyu He[2#], Yunfei Zhao[1,2#], Gang Zou[2], Mengjiao Deng[2], Liming Yang[2], Ke Hu[1], Yaxi Chen[1], Yu Chao[2*]*

[1] Centre for Lipid Research & Chongqing Key Laboratory of Metabolism on Lipid and Glucose, Key Laboratory of Molecular Biology for Infectious Diseases (Ministry of Education), the Second Affiliated Hospital, Chongqing Medical University, 400016, Chongqing, China

[2] Chongqing Medical University, College of Pharmacy, Chongqing Key Laboratory for Pharmaceutical Metabolism Research, Chongqing Pharmacodynamic Evaluation Engineering Technology Research Center, Chongqing 400016, P. R. China

***** Corresponding authors.

E-mail addresses: chenyaxi@cqmu.edu.cn; yuchao@cqmu.edu.cn.

[#] These authors contributed equally to this work.

ABSTRACT

Mixed hyperlipidemia is characterized by concurrent hypercholesterolemic and hypertriglyceridemic burdens, which cannot be adequately addressed by existing single-target lipid-lowering strategies, leaving patients with considerable residual cardiovascular risk. Herein, we developed a single dual-target rAAV carrying a dual-promoter cassette simultaneously silences PCSK9 and APOC3, and established an optimized triple-plasmid packaging strategy to overcome the bottleneck imposed by its large (~5.3 kb) cargo. Systematic titration of the three packaging plasmids identified a three-fold increase in pHelper dosage as the optimal balance of replication and packaging resources, which elevated viral yield, restored the canonical 1:1:10 capsid stoichiometry, and markedly reduced the empty-capsid fraction.In a high-fat-diet mouse model, a single administration of this dual-target rAAV concurrently knocked down hepatic PCSK9 and APOC3, reducing serum TC by approximately 30% and TG by approximately 70%, with an approximately 40% gain in editing efficiency over the unoptimized vector. Moreover, this optimized dual-target rAAV offered superior advantages over single-target AAV in ameliorating systemic energy metabolic phenotypes, manifested as increased energy expenditure and a reduced respiratory exchange ratio. Overall, this study provides a feasible strategy for producing large-cargo dual-target rAAVs and establishes proof-of-concept for single-administration, dual-target gene therapy against mixed hyperlipidemia.

INTRODUCTION

Mixed hyperlipidemia is characterized by concomitant elevations in serum total cholesterol (TC) and triglycerides (TG). Familial combined hyperlipidemia is a genetically influenced phenotype with a predominantly polygenic basis that is also shaped by metabolic and environmental factors[1, 2]. This lipid profile constitutes a major risk factor for atherosclerotic cardiovascular disease (ASCVD), which remains the leading cause of mortality worldwide [3, 4]. Despite the availability of statins, inclisiran, ezetimibe and other lipid or cholesterol lowering pharmacotherapies, patients with mixed hyperlipidemia continue to exhibit considerable residual cardiovascular risk [5].This clinical gap arises because cholesterol and triglyceride metabolism are governed by distinct yet complementary pathways, and no single-target therapy concurrently addresses both arms of the disease, underscoring the pressing need for an intervention that tackles the hypercholesterolemic and hypertriglyceridemic components in parallel.

Two of the most compelling gene targets for this dual burden are proprotein convertase subtilisin/kexin type 9 (PCSK9) and apolipoprotein C3 (APOC3). The former impedes LDL-C clearance by promoting low-density lipoprotein receptor (LDL-R) degradation, whereas the latter reduces triglyceride hydrolysis from TG rich lipoproteins via LPL inhibition and impairs remnant uptake, positioning APOC3 as a key negative regulator of TG metabolism [6, 7]. Targeting PCSK9 therefore unblocks the cholesterol-clearance pathway, while silencing APOC3 restores the triglyceride-clearance. the two genes thus act as naturally complementary nodes of one metabolic axis, providing a mechanistic rationale for their co-targeting within a single therapeutic agent.

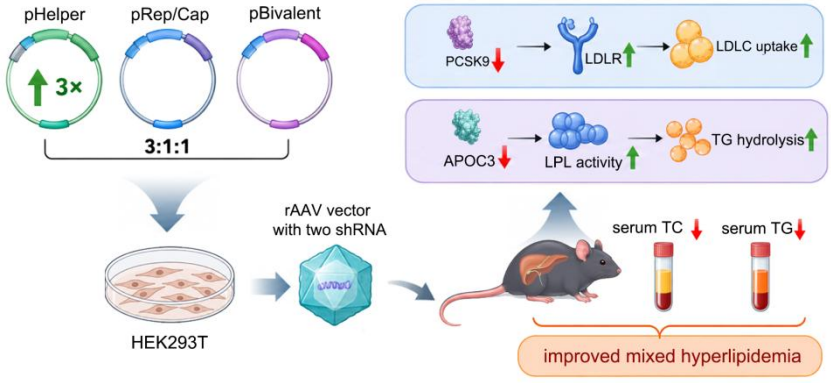
Management of mixed hyperlipidemia typically relies on a combination of multiple lipid-lowering agents [8]. This approach is complicated by drug interactions, increased hepatic burden, and suboptimal patient adherence due to missed doses from complex, multi-daily dosing regimens [9]. Recently, multi-targeting via a single therapeutic agent has attracted considerable attention. ARO-DIMER-PA, for instance, covalently links two independent RNAi molecules within a single construct and represents a clinical candidate capable of dual-gene silencing from a single molecule, thereby demonstrating the feasibility of modulating two distinct pathways with one agent [10]. While this paradigm highlights the potential of multi-target strategies, it also underscores the urgent need for more comprehensive, complementary, and durable gene-based therapeutic alternatives.

However, RNAi-based silencing is inherently transient, and the promise of a durable, single-administration, dual-gene intervention remains unmet. Notably, given that rAAV vectors have demonstrated favorable safety, transduction efficiency, and sustained expression in single-gene targeting [11], we asked whether such vectors could be engineered to simultaneously target multiple lipid metabolic pathways while preserving these advantages.

Although the concept of a single dual-targeting rAAV is attractive, its implementation poses significant technical challenges. Conventional strategies, including the use of internal ribosome entry sites (IRES) or 2A peptides, often lead to imbalanced expression of the downstream gene [12]. An alternative approach employing two independent promoters within a single vector affords independent regulation of each transgene but imposes a substantial cargo size burden [13]. For example, in the present study, the size of the PCSK9/APOC3 transgenic cassette (~5.3 kb) approaches the packaging capacity limit of rAAV, which may compromise packaging efficiency, increase empty capsid ratios, and further constrain industrial-scale production and clinical translation of rAAV-based therapies. Previous studies have demonstrated that optimization of the composition and stoichiometry of the triple-plasmid system can significantly enhance the production efficiency of single target rAAV [14]. The triple-plasmid system consists of a transgene plasmid flanked by inverted terminal repeats (ITRs), a Rep/Cap plasmid encoding AAV replication and capsid genes, and a helper plasmid providing adenoviral auxiliary functions. The transgene plasmid carries the expression cassette of interest, the Rep/Cap plasmid supplies the AAV replication proteins and structural capsid proteins, and the helper plasmid provides auxiliary functional proteins to create a favorable environment for viral replication. The stoichiometric ratios among the three plasmids critically influence packaging efficiency: an excessive proportion of the transgene plasmid competitively consumes auxiliary protein resources, leading to reduced genome replication efficiency [15, 16]; an overabundance of the Rep/Cap plasmid, although enhancing capsid protein expression, may suppress host cell growth due to excess Rep proteins, thereby diminishing overall yield [17]; and insufficient helper plasmid fails to provide adequate auxiliary functions, resulting in impaired AAV gene expression and replication [18]. Through systematic optimization of the three-plasmid ratios, resource competition among plasmids can be balanced, maximizing the production of intact viral particles and enabling precise modulation of both rAAV production efficiency and

empty capsid ratios [15]. To the best of our knowledge, however, optimization of the ratios of the triple-plasmid system specifically tailored for large dual-promoter constructs has not been extensively explored [16].

Herein, we hypothesized that optimization of the plasmid ratios within the triple-plasmid transfection system would enable efficient packaging of a ~5.3 kb dual-promoter expression cassette encoding PCSK9 and APOC3 targeting sequences. In vivo, this optimized single-vector rAAV concurrently silenced hepatic PCSK9 and APOC3, resulting in approximately 30% and 70% reductions in serum TC and TG, respectively (**Scheme.1**). Collectively, this study not only provides a feasible process optimization strategy for the scalable production of dual-targeting single-vector rAAVs but also establishes proof-of-concept for a single administration, dual-target gene therapeutic approach for mixed hyperlipidemia.



Scheme.1 An optimized triple-plasmid system enables efficient production of a single dual-target rAAV co-delivering shPcsk9 and shApoc3. This vector simultaneously silences hepatic PCSK9 and APOC3, upregulates LDLR and LPL activity, and ameliorates mixed hyperlipidemia in mice.

METHODS

Materials and Instrument

Materials： Fetal bovine serum (Gibco, US), pAAV-U6-shRNA1-ZsGreen1 plasmid (Miaolin, Wuhan, China), BamHI restriction enzyme and HindIII restriction enzyme (Thermo, US), T4 DNA ligase (shenggong, shanghai, China), Gel-red dye (Takara, Japan), DNA Marker (Takara, Japan), 2×Taq Master Mix (Novazan, China), Iodixanol (Serumwerk Bernburg AG), DNA ladder (Takara, Japan), Alanine aminotransferase Assay Kit (C009-2-1), Aspartate aminotransferase Assay Kit

(C010-2-1), Proprotein convertase subtilisin/kexin type 9 (H430-1-1), ELISA Kit for Apolipoprotein C3 (APOC3) (SEB89OMu), Creatinine (Cr) Assay Kit (sarcosine oxidase) (C011-2-1), Urea Assay Kit (C013-2-1), Low-density lipoprotein cholesterol assay kit (A113-1-1), High-density lipoprotein cholesterol assay kit (A112-1-1), Total cholesterol assay kit (A111-1-1), Triglyceride assay kit (A110-1-1), Lipoprotein lipase, Hepatic Lipase assay kit (A067-1-2)

Instruments: QuantStudio 3 Real-Time Fluorescent Quantitative PCR System (Thermo, US), Gel Imaging System (Bio-Rad, USA), Ultra-Speed Centrifuge (Thermo, US), NanoDrop UV Spectrophotometer (Bording, France), Electrophoresis System and Blotting Apparatus (Bio-Rad, USA), Tanon 5200 Chemiluminescence Imaging System (Tianneng, shanghai, China), PCR Amplifier (Bio-Rad, USA), Labsystems Multiskan MS Microplate Reader (Thermo, US), Leica Upright Fluorescence Microscope (Thermo, US), METTLER TOLEDO MS-TS Analytical Balance (Mettler-Toledo, shanghai, China)

Cell culture

Human hepatocellular carcinoma cells (HepG2) and human embryonic kidney cells (HEK293T) were obtained from Punosai (Wuhan, China). All cell lines were maintained in a humidified incubator at 37 °C with 5% CO_2. HepG2 cells were cultured in Dulbecco's modified Eagle's medium (DMEM; 4.5 g/L glucose; BasalMedia, Shanghai, China) supplemented with 10% heat-inactivated fetal bovine serum (FBS), 1× non-essential amino acids, and penicillin–streptomycin. Cells were passaged at a 1:3 ratio every other day. For transfection experiments, HepG2 cells were seeded into six-well plates at 1×10^6 cells per well and transduced at the indicated multiplicity of infection (MOI). HEK293T cells used for rAAV packaging were cultured in the same complete DMEM medium. Before transfection, HEK293T cells were seeded into 10-cm culture dishes and transfected at approximately 80% confluence using PEI-mediated triple-plasmid co-transfection. All cell lines were regularly tested for mycoplasma contamination to avoid experimental interference.

Mice

Thirty 8-week-old male C57BL/6J mice were selected for the study. All mice were fed a high-fat diet (HFD) to establish the relevant disease models. After 7 weeks of HFD feeding, mice were administered treatments via tail vein injection and assigned to the following groups (6 mice per

group): normal control (NC, fed a normal diet, no viral treatment), negative control group (rAAV-shNC), experimental group 1 (rAAV-sh*Pcsk9*), experimental group 2 (rAAV-sh*Apoc3*), and experimental group 3 (rAAV-sh*Pcsk9*-sh*Apoc3*). At week 10, key organs including the heart, liver, spleen, lungs, and kidneys were collected for HE staining to examine potential pathological changes. Additionally, blood was collected from the mice's eyeballs, and serum was separated by centrifugation for the analysis of biochemical indicators.

Ethical Approval

All experimental animals were purchased from the Experimental Animal Center of Chongqing Medical University. All procedures and protocols involving animal experiments were reviewed and approved by the Animal Ethics Committee of Chongqing Medical University. All animal experiments were conducted in the IVC (Individually Ventilated Cage) animal facility of the Experimental Animal Center of Chongqing Medical University. The entire experimental process strictly adhered to the “Regulations on the Administration of Laboratory Animals” and the requirements of animal ethics review to ensure the standardization and scientific validity of the experimental operations.

Construction and Transformation of shRNA Plasmid

Synthesis of shRNA interference plasmids. The Gene ID of the target human gene was retrieved from the 'Gene' database of the National Center for Biotechnology Information (NCBI). Subsequently, the BROAD Institute website was utilized to select shRNA core sequences with high prediction scores. Following established shRNA primer design principles, primers were designed and synthesized by shenggong Biotech. After primer annealing, the pAAV-U6 vector was selected as the backbone and linearized using the restriction enzymes BamHI and HindIII. The annealed oligonucleotides were ligated into the digested vector to construct the knockdown plasmid.

Plasmid transformation and extraction. The ligation product was transformed into Stbl3 competent cells. Briefly, a tube of Stbl3 E. coli (Miaolin , Wuhan , China) was thawed on ice, and 4.5 μL of the ligation product was added. The mixture was incubated on ice for 30 min, followed by heat shock at 42 °C for 60 s and immediate chilling on ice for 2 min. Subsequently, 500 μL of antibiotic-free LB medium was added, and the culture was shaken at 180 rpm for 45 min. The culture was

centrifuged at 4000 rpm for 1 min, the supernatant was partially removed, and the pellet was resuspended in the remaining 50-100 μL. The resuspended cells were spread onto LB agar plates containing ampicillin, incubated upright for 30 min, and then inverted for incubation at 37 °C for 12-14 h. A single colony was picked into LB liquid medium containing ampicillin and shaken at 180 rpm for 14-16 h. Plasmids were extracted using the TienGen Biotech high-purity, endotoxin-free plasmid min/maxiprep kit (DP118) according to the manufacturer's instructions.

Plasmid Identification. Positive clones yielding DNA fragments of the expected size were selected for glycerol stock preservation and sent to shenggong Biotech for sequencing validation.

Virus production

HEK293T cells were seeded into 10-cm culture dishes and transfected when confluence reached approximately 80%. The pAAV-shRNA, pHelper, and pAAV-RC plasmids were mixed at a 1:1:1 ratio in 100 μL of serum-free medium and incubated at room temperature for 5 min. PEI solution was then added at a plasmid-to-PEI mass ratio of 1:3 (1 μg/μL), and the mixture was incubated at room temperature for 10–15 min. The plasmid–PEI complexes were added to each 10-cm dish, gently mixed, and returned to a 37 °C incubator. At 5–6 h after transfection, the medium was replaced with fresh complete medium supplemented with 10% fetal bovine serum (FBS).

Optimization of the triple-plasmid packaging system

To optimize rAAV production and the empty-to-full capsid ratio, the relative amounts of the three plasmids were systematically varied. For each target plasmid, its amount was tested at ratios of 0.3:1:1, 1:1:1, 3:1:1, and 10:1:1 against the other two plasmids. HEK293T cells were seeded in six-well plates at 1×10^6 cells per well and transfected with pAAV-shRNA, pHelper, and pAAV-RC (pAAV-RC was obtained from Wuhan Miaolin Biotechnology Co., Ltd., Wuhan, China) according to the indicated ratios. The culture medium was replaced with fresh complete medium 5–6 h after transfection. Cell viability and genomic titers were assessed at 24, 48, 72, 96, and 120 h post-transfection. Transfection efficiency was evaluated by monitoring green fluorescence intensity using high-content fluorescence microscopy. Cell viability was measured using the CCK-8 assay, and viral genomic titers were determined by quantitative PCR (qPCR).

CCK-8 cell viability assay

At 24, 48, 72, 96, and 120 h after triple-plasmid transfection, the culture medium was replaced with 1.8 mL of fresh complete medium containing 200 μL of CCK-8 reagent (Beyotime, Shanghai, China; medium:CCK-8 = 9:1, v/v). Cells were incubated at 37 °C in a humidified incubator for 60 min. Absorbance at 450 nm was measured using a microplate spectrophotometer (Agilent, Santa Clara, CA, USA). Relative cell viability was calculated by normalizing the optical density values to those of the control group.

Determination of viral titer

At different time points after transfection, 20 μL of harvested supernatant was treated with 0.2 μL of DNase I at 37 °C for 30 min. Then, 10 μL of the reaction mixture was transferred to a new tube, mixed with 2 μL of EDTA, and incubated at 65 °C for 10 min to inactivate DNase I. Subsequently, 2 μL of proteinase K and 36 μL of nuclease-free water were added, and the samples were incubated at 50 °C for 20 min, followed by heat inactivation at 95 °C for 15 min. Viral genomic titers were quantified by qPCR using primers targeting ZsGreen1 or APOC3 sequences present in the rAAV-shRNA vector.

Virus harvest and pre-purification processing

At 48 h post-transfection, culture dishes were removed, and the supernatants were collected. The cell monolayers were washed three times with phosphate-buffered saline (PBS). Cells were harvested and resuspended in AAV lysis buffer (150 mM NaCl, 50 mM Tris, pH 8.4). The cell suspension and the original culture supernatant were combined in 50-mL centrifuge tubes and centrifuged at 2,000 × g for 20 min. The supernatant was discarded, and the cell pellet was resuspended in AAV lysis buffer. Cell lysates were subjected to three freeze–thaw cycles (37 °C water bath followed by liquid nitrogen), with each cycle lasting approximately 2 min. The crude lysates were then treated with benzonase (10 U per mL of lysate) at 37 °C for 30 min. Cellular debris was removed by centrifugation at 1,600 × g for 5 min at room temperature, followed by centrifugation at 16,600 × g for 10 min at 4 °C. The clarified supernatants were collected for subsequent purification.

rAAV-shRNA Virus Purification Using Iodixanol Density Gradient Centrifugation

Solution Preparation and Sample Loading: Solutions of 10× PBS-MK, PBS-MK, and PBS-MKN

were prepared. Iodixanol solutions of 54%, 40%, 25%, and 15% were prepared using OptiPrep (60% iodixanol). Phenol red solution (0.01 μg/mL) was added to the 25% and 54% solutions.

Gradient Centrifugation: Using a loading needle, the iodixanol solutions were carefully layered from bottom to top in an ultracentrifuge tube as follows: 1 mL of 54% iodixanol (with phenol red), 1 mL of 40% iodixanol, 1.2 mL of 25% iodixanol (with phenol red), and 1.8 mL of 15% iodixanol. The pretreated sample was gently layered on top until the tube was full. Ultracentrifugation was performed at 350,000 g (64,000 rpm) at 18 °C for 1 h. Following centrifugation, an 18-gauge needle was used to puncture the tube just below the interface to collect the viral fraction into an Eppendorf tube.

Dialysis: A dialysis membrane with a 10 kDa molecular weight cutoff was prepared. The purified virus solution was loaded into the membrane, which was then clamped at both ends and placed in a beaker containing fresh PBS. Dialysis was performed at 4 °C on a magnetic stirrer, with the PBS being replaced every 4 h for a total of three exchanges.

Concentration: The sample was concentrated using a UFC810096 ultrafiltration tube (MWCO 100 kDa). A maximum of 4 mL of sample was added to the tube, which was then centrifuged at 4000 rpm for 40 min. The concentrated sample was filtered through a 0.22 μm sterile microporous membrane, collected, and stored at -20 °C or -80 °C.

Viral transduction

HepG2 cells were seeded into six-well plates and transduced when confluence reached approximately 80%. The required amount of viral vector (vg) was calculated as MOI (vg per cell) × number of cells. The MOI was selected according to the manufacturer's instructions for the transduction reagent. The viral suspension was added to each well of the six-well plate, gently mixed, and returned to a 37 °C incubator for continued culture. At 6-12h after transduction, the medium was replaced with fresh complete medium containing 10% FBS. Functional assays were performed 48 h post-infection.

Quantitative real-time PCR

Total RNA was extracted from mouse liver tissues and cultured cells. RNA concentration and purity

were quantified, and RNA was reverse-transcribed into cDNA. Quantitative real-time PCR was performed using a real-time PCR system (Thermo Fisher Scientific, Waltham, MA, USA). The relative expression levels of target genes were calculated using the 2−ΔΔCT method. **Western Blot**

Total proteins were extracted from mouse liver tissues and cultured cells. Protein samples were separated by SDS-PAGE (90 V for 30 min, then 120 V for 90 min) and subsequently transferred onto a membrane (constant current of 250 mA in an ice bath; transfer time was determined according to the protein molecular weight). After blocking with a rapid protein blocking solution for 20 min, the membrane was incubated with the primary antibody overnight at 4 °C. Anti-LDL-R antibody (ab52818, Abcam, UK), Anti-PCSK9 antibody (ab185194, Abcam, UK), Anti-VP1/VP2/VP3 antibody (Bo'ao Long, Suzhou, China) ,Anti-APOC3 antibody (ab76305, Abcam, UK). The following day, after incubation with the corresponding secondary antibody (Sanying, Wuhan, China), protein signals were detected using an electrochemiluminescence imaging system (shenhua, shanghai, China).

Coomassie Brilliant Blue Staining

Protein samples were resolved by SDS-PAGE under constant voltage conditions (80 V for 30 min, followed by 120 V for 90 min). The gel was subsequently immersed in Coomassie Brilliant Blue staining solution (P0003S, Beyotime, China) to ensure complete coverage and incubated at room temperature for 1 h. Following incubation, the staining solution was discarded, and the gel was destained in ddH_2O with gentle agitation. The destaining solution was replaced 4–8 times until the background was sufficiently cleared and protein bands were clearly visualized. The gel was then imaged for analysis.

Oil Red O Staining

HepG2 cells were seeded at 60% confluency onto 6-well plates containing coverslips and cultured for 48 h, followed by 24 h of serum starvation. The medium was replaced with serum-free DMEM containing 50 μg/mL LDL-C and incubated for 24 h. The supernatant was discarded, and the coverslips were rinsed three times with pre-cooled PBS (pH 7.4) for 3 min each. Cells were fixed with 300 μL of 4% paraformaldehyde at room temperature for 15 min. After washing three times with PBS, cells were stained with 300 μL of modified Oil Red O working solution (C0157S,

Beyotime, China) in the dark for 30 min. The dye was discarded, and the wells were washed gently three times with PBS. Nuclei were counterstained with 300 μL of hematoxylin solution for 1-2 min at room temperature, followed by three washes with PBS. The coverslips were removed and mounted with a small amount of glycerol.

Total Cholesterol (TC) and Triglyceride (TG) Quantification

To the collected cell pellets, 0.2-0.3 mL of homogenization medium (0.1 mol/L phosphate buffer, pH 7.0-7.4) was added. The mixture was gently pipetted, and the tube was placed in an ice-water bath. Cells were lysed by sonication, incubated at 37 °C for 10 min, and the absorbance was measured at 500 nm using a microplate reader. A standard curve was plotted for content calculation.

ELISA

Set up wells, and sequentially add 100 μL of standard solutions at different concentrations. Add 100 μL of standard solution diluent to the blank well, and add 100 μL of the sample to the remaining wells. Cover the microplate and incubate at 37°C for 1 hour. Discard the liquid, flick dry without washing. Add 100 μL of working solution A to each well, cover the microplate, and incubate at 37°C for 1 hour. Discard the liquid in the wells, wash each well with 350 μL of washing solution, soak for 1-2 minutes, and gently tap the microplate on absorbent paper to remove all liquid from the wells. Repeat the washing step 3 times. After the final wash, aspirate or pour out the remaining wash buffer, invert the microplate onto absorbent paper, and remove all residual liquid in the wells. Add 100 μL of working solution B to each well, cover the microplate, and incubate at 37°C for 30 minutes. Discard the liquid in the wells, flick dry, and wash the plate 5 times. Add 90 μL of TMB substrate solution to each well, cover the microplate, and incubate at 37°C protected from light to develop color. Add 50 μL of stop solution to each well to terminate the reaction; the blue color turns yellow immediately. Measure the optical density of each well at a wavelength of 450 nm immediately.

Off-target effect

Potential off-target effects of the candidate shRNA sequences (shPcsk9 and shApoC3) were predicted through an in silico analysis using the NCBI Nucleotide BLAST (BLASTn) algorithm. Candidate off-target genes were ranked according to the number and position of mismatches, with priority given to those containing seed-region matches and those with complementarity at the 3′ end

of the seed region, as these are most likely to be incorporated into the RNA-induced silencing complex (RISC) and mediate unintended silencing. The top-scoring candidate off-target genes for PCSK9 (SORCS1, TMKS, OR5B17) and APOC3 (SMG9, TSPAN14, HKDC1) were selected for experimental validation.

Hematoxylin and Eosin (H&E) Staining

Mouse liver tissues were harvested after euthanasia and fixed in 4% paraformaldehyde for 24 h at room temperature. Fixed samples underwent gradient ethanol dehydration, xylene clearing and paraffin embedding. Tissue blocks were cut into 4–10 μm continuous slices, followed by standard H&E staining procedures (C0105S, Beyotime, China) .After sealing with neutral mounting medium, histological sections were visualized under light microscopy at multiple magnifications to evaluate hepatocyte injury, inflammatory infiltration and overall hepatic tissue morphology.

Metabolic cage

Whole-body metabolic phenotypes were evaluated using a CLAMS indirect calorimetry metabolic cage system. Mice were individually housed in sealed metabolic chambers with unrestricted access to food and water. Mice were acclimated to the cage environment for 48 h before continuous data acquisition over 24 consecutive hours under a standardized 12 h light/dark photoperiod at 25 °C. Real-time parameters including total energy expenditure (EE), respiratory exchange ratio (RER), cumulative food/water intake were recorded at 15 min intervals.

Statistical Analysis

Statistical differences between groups were determined using two-tailed t-tests (and non-parametric tests where appropriate). Statistical analyses were performed with GraphPad Prism 8.0.2. Data are presented as mean ± standard error. P values are indicated as *P < 0.05, **P < 0.01, ***P < 0.001, ****P < 0.0001; ns indicates no significant difference.

RESULTS

Construction and Characterization of rAAV-sh*Pcsk9*-sh*Apoc3*

The sequence of the bivalent shRNA plasmid is shown in **Figure.1a**. This construct simultaneously carries shRNA sequences targeting PCSK9 and APOC3, both of which were identified as high-

scoring core sequences screened from the BROAD website. The pAAV-U6 vector was selected as the backbone, and the shRNA sequences were cloned into the pAAV-U6 backbone via the BamHI/HindIII restriction endonuclease sites located downstream of the U6 promoter within the ITR expression cassette. Each shRNA expression cassette was driven by an independent U6 promoter to ensure that transcriptional activities would not interfere with one another; this strategy has been previously demonstrated to achieve stable and sustained gene silencing in mammalian cells [19]. Sanger sequencing confirmed the correct insertion of both hairpin sequences, with alignment results completely matching the expected design (**Figure.1a**).

After co-transfection of the three plasmids into 293T cells using the three-plasmid co-transfection system, recombinant AAV particles were packaged and subsequently used to infect HepG2 cells, followed by RT-qPCR analysis to assess gene silencing efficiency. As illustrated in **Fig. 1b,** the bivalent construct produced markedly lower viral titers than the monovalent vector, and a substantial proportion of particles appeared to be empty or packaging-defective. Consistent with this, the bivalent rAAV-shPcsk9-shApoc3 reduced both PCSK9 and APOC3 mRNA levels by only approximately 30%, confirming successful construction of the dual-targeting vector but indicating that the knockdown efficiency was limited by packaging defects rather than by the shRNA sequences themselves (**Fig. 1b**). We therefore further characterized the physicochemical properties of the bivalent rAAV vector, hypothesizing that the reduced efficiency originated from viral packaging defects rather than from the shRNA sequences themselves. SDS-PAGE analysis of the capsid proteins revealed three distinct bands at approximately 90 kDa (VP1), 72 kDa (VP2), and 60 kDa (VP3), confirming the presence of all three structural proteins. However, densitometric quantification yielded a VP1:VP2:VP3 ratio of 34.02%:29.69%:36.29%, which deviated substantially from the canonical stoichiometry of 1:1:10 (**Figure.1c, Fig.S6**). Transmission electron microscopy (TEM) was then employed to examine the morphology of the rAAV-sh*Pcsk9*-shApoc3 viral particles, and numerous collapsed empty capsids were observed (**Figure.1d**). Finally, comparative analysis of the relative viral titers between bivalent and monovalent rAAV vectors demonstrated that the bivalent viral titer was significantly lower than that of the monovalent virus (**Figure.1e**). These results indicate that introduction of the dual shRNA expression cassette reduces viral packaging efficiency.

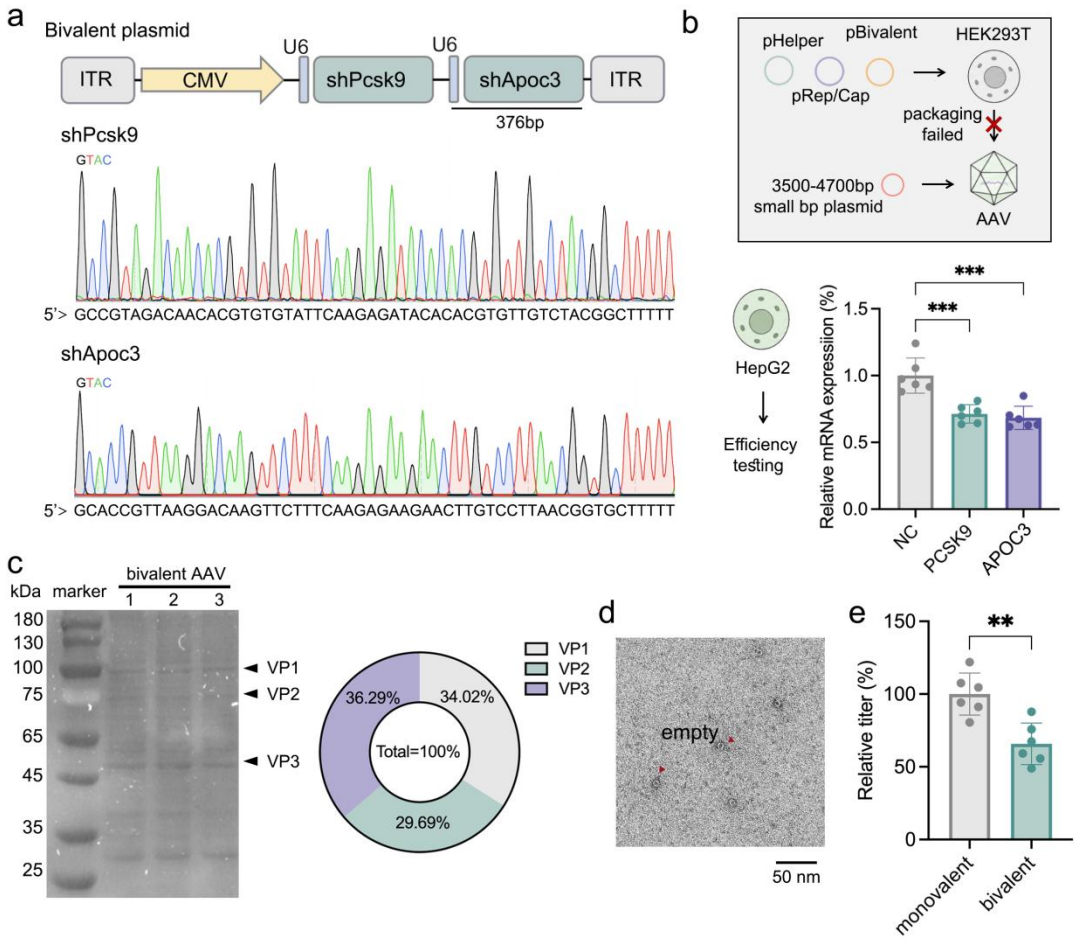


Fig.1 Construction and Characterization of rAAV-sh*Pcsk9*-sh*Apoc3*. a Schematic of the dual-target shRNA plasmid carrying sh*Pcsk9* and shApoc3 sequences. Proper insertion of each hairpin was confirmed by sequencing alignment. **b** Schematic of the standard three-plasmid co-transfection system and assessment of packaging and silencing efficiency. The bivalent construct exhibited impaired packaging and a higher proportion of empty capsids, and reduced both PCSK9 and APOC3 mRNA levels in HepG2 cells. **c** SDS-PAGE analysis of rAAV-sh*Pcsk9*-shApoc3 particles and stoichiometry of capsid VP1, VP2 and VP3 proteins. **d** TEM showing the morphology of rAAV-sh*Pcsk9*-shApoc3 virions; scale bar = 50 nm. **e** Comparison of relative viral titers of bivalent versus monovalent rAAV.*P < 0.05; **P < 0.01; ***P < 0.001.

Optimization of the Bivalent Packaging System

Optimization of the three-plasmid system can improve transgene expression and viral packaging efficiency, providing a basis for scalable rAAV production. To further enhance yield and optimize the packaging process, we constructed a modified bivalent plasmid carrying the ZsGreen1 green fluorescent reporter gene, whose fluorescence intensity allows direct visualization of transfection

efficiency (**Figure.2a**). HEK293T cells transfected with different three-plasmid ratios (pHelper:pRepCap:pBivalent) were imaged under a high-content fluorescence microscope, and ZsGreen1-positive cells were used as an indicator to evaluate transfection efficiency (**Figure.2b**). The plasmid ratios were systematically increased in a geometric progression to evaluate the impact of the three-plasmid ratios on packaging efficiency. Quantitative analysis using relative fluorescence intensity as the primary metric revealed that the 3:1:1 ratio yielded a mean fluorescence intensity significantly higher than that of all other experimental groups (**Figure.2c–e**). This indicates that this specific ratio achieves relatively favorable transgene expression and viral packaging efficiency, providing more advantageous packaging conditions for subsequent studies.

Physicochemical Characterization of the Optimized Bivalent AAV-sh*Pcsk9*-sh*Apoc3*

Viral genome titers in HEK293T cells were measured by RT-qPCR at multiple time points post-transfection (24, 48, 72, 96, and 120 h). The viral genome titer peaked at 48 h post-transfection, reaching approximately 3×10^{11} VG/mL, thereby establishing 48 h as the standard harvest time point for subsequent experiments (**Figure.2f**). We also evaluated the effect of viral production at different time points (hours) on cell viability. Cell viability was assessed by CCK-8 assay at the same time points, showing a time-dependent decline from approximately 90% at 24 h to approximately 40% at 120 h post-transfection, with cell viability remaining above 90% at the optimal harvest time point of 48 h (**Figure.S1**). Under the optimized three-plasmid ratio, Western blot analysis confirmed that the stoichiometry of the capsid proteins (VP1, VP2, and VP3) in the prepared rAAV particles conformed to the expected 1:1:10 ratio (**Figure.2g, Fig.S6**). Furthermore, TEM micrographs of the rAAV-sh*Pcsk9*-shApoc3 particles produced under these optimized packaging conditions showed that the majority of particles exhibited an intact, fully encapsidated morphology with a diameter of approximately 25 nm (**Figure.2h**). Compared with the unoptimized preparation shown in Figure.1, the optimized system restored the canonical VP1:VP2:VP3 stoichiometry, converted the predominantly collapsed/empty capsids into intact particles, and raised the viral genome titer, a level comparable to that routinely obtained for the monovalent vectors. These comparisons indicate that the three-fold increase in pHelper dosage effectively closed the gap between the bivalent and monovalent vectors.

In summary, by evaluating different plasmid ratios and measuring viral titers at multiple time points

post-transfection, we systematically determined the optimal pHelper:pRep/Cap:pBivalent ratio and the optimal harvest time for viral production. The optimized formulation improved the packaging efficiency of the bivalent rAAV vector and providing more reliable packaging conditions for subsequent functional validation.

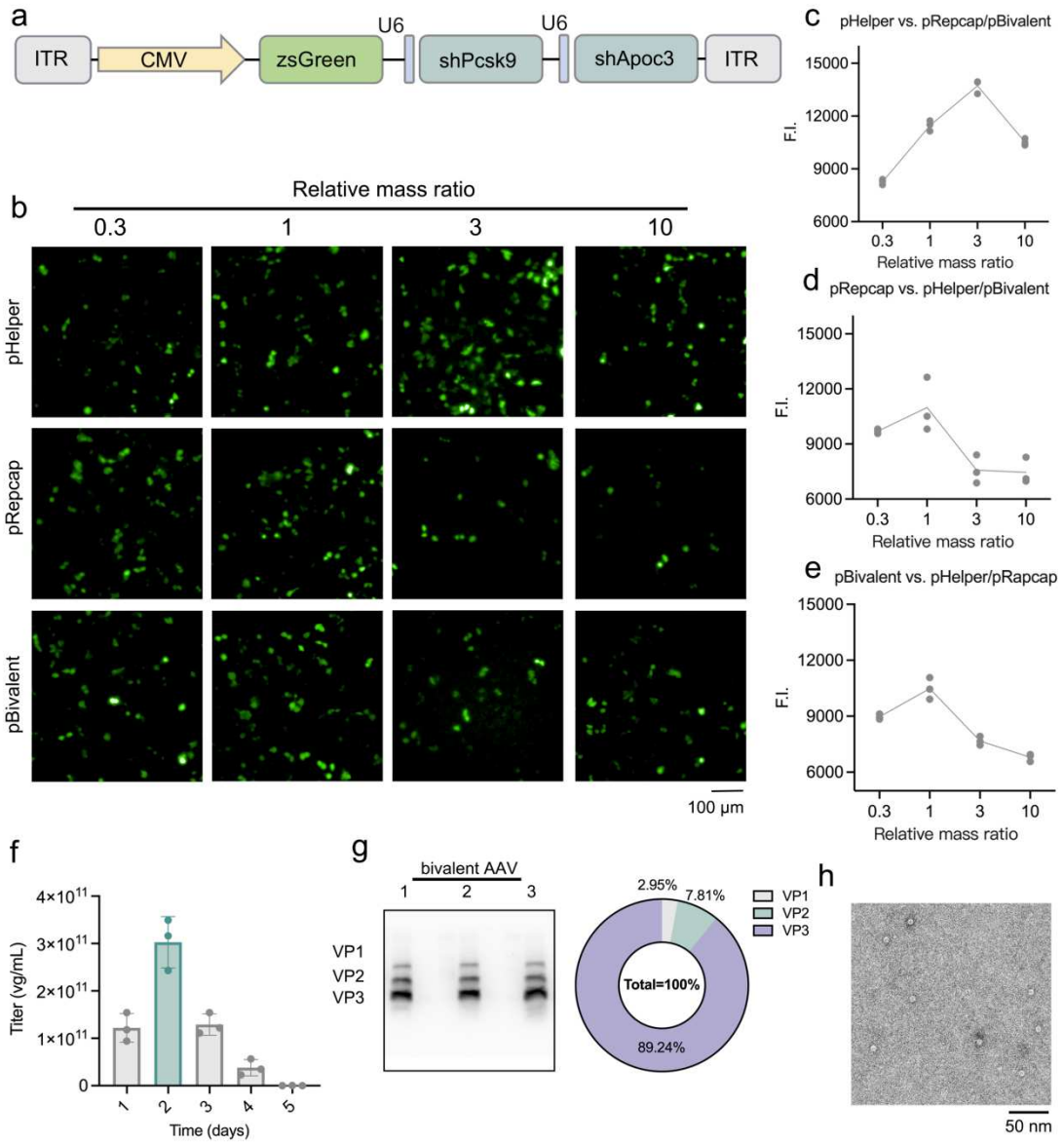


Fig.2 Optimization of the Bivalent Packaging System. Physicochemical Characterization of the Optimized Bivalent AAV-sh*Pcsk9*-sh*Apoc3*. **a** Schematic and characterization of the dual-target plasmid and packaged rAAV. (a) Schematic diagram of the modified dual-target plasmid incorporating the ZsGreen1 green fluorescent reporter gene cassette. **b** Representative high-content fluorescence microscopy images (40×) of HEK293T cells transfected with three-plasmid packaging systems at different ratios; ZsGreen1-positive cells served as an indicator of

transfection efficiency. **c-e** Quantification of packaging efficiency in HEK293T cells under different three-plasmid ratios, presented as relative fluorescence intensity. **f** RT-qPCR analysis of viral genomic titers at different time points post-transfection in HEK293T cells. **g** SDS-PAGE verification of the ratios of capsid proteins VP1, VP2 and VP3 in rAAV particles produced under the optimized three-plasmid ratio. **h** TEM micrographs of rAAV-sh*Pcsk9*-shApoc3 viral particles generated under optimized packaging conditions; scale bar = 50 nm.

In Vitro Knockdown and Functional Validation of the Bivalent AAV-sh*Pcsk9*-sh*Apoc3*

In vitro experimental workflow is illustrated in **Figure.3a**, HepG2 cells were seeded and treated with NC, rAAV-shNC, rAAV-shPcsk9, rAAV-shApoc3, or the bivalent rAAV particles, followed by analysis at the indicated time points. RT-qPCR analysis of HepG2 cells treated in vitro with NC, rAAV-shNC, rAAV-sh*Pcsk9*, rAAV-shApoc3, or the bivalent rAAV particles revealed that treatment with the bivalent vector significantly reduced PCSK9 mRNA levels and APOC3 mRNA levels (by approximately 80%) (**Fig. 3b**). The knockdown efficiency was comparable to that of the corresponding monovalent vectors, confirming the functional independence of the two shRNA expression cassettes. Quantitative Western blot analysis further validated these results at the protein level (**Fig. 3c–f, Fig.S7**). PCSK9 protein levels were significantly reduced in both the rAAV-sh*Pcsk9* group and the bivalent vector group, accompanied by a significant upregulation of LDL-R expression, which is consistent with the established mechanism by which PCSK9 inhibition prevents LDL-R degradation [7]. Treatment with rAAV-shApoc3 significantly decreased APOC3 protein levels without affecting the expression levels of PCSK9 or LDL-R. The bivalent vector group maintained knockdown levels equivalent to those of the monovalent vectors.

The metabolic rationale for dual targeting lies in the distinct roles of PCSK9 and APOC3 in lipid homeostasis. PCSK9 promotes the degradation of the LDL-R in hepatocytes, thereby reducing the clearance of circulating LDL-C [8], whereas APOC3 inhibits the activity of LPL, thereby impairing hepatic uptake of triglyceride-rich lipoprotein remnants [6]. These two pathways constitute complementary nodes in lipid metabolism, and simultaneous intervention can achieve more pronounced lipid-lowering effects. A schematic diagram of this synergistic mechanism is shown in **Figure.3g**. The bivalent rAAV-sh*Pcsk9*-shApoc3 group further exacerbated lipid accumulation, with larger and more densely distributed lipid droplets, suggesting that APOC3 knockdown exerts a synergistic effect by additionally regulating intracellular lipid metabolism. Consistent with

enhanced LDL-C uptake, intracellular TC levels were significantly elevated in both the rAAV-sh*Pcsk9* and bivalent groups (**Fig. 3h**). However, under basal culture conditions, no significant differences in intracellular TG levels were observed among the treatment groups (**Fig. 3i**), indicating that APOC3 knockdown mediated TG regulation may require an in vivo metabolic environment, specifically one involving LPL activity and lipoprotein metabolism, to be fully realized. Oil Red O staining was futher performed to assess intracellular lipid accumulation. The rAAV-sh*Pcsk9* treatment group exhibited a marked increase in the number of lipid droplets due to enhanced uptake of exogenous LDL-C via upregulation of LDL-R (**Fig. 3j**).

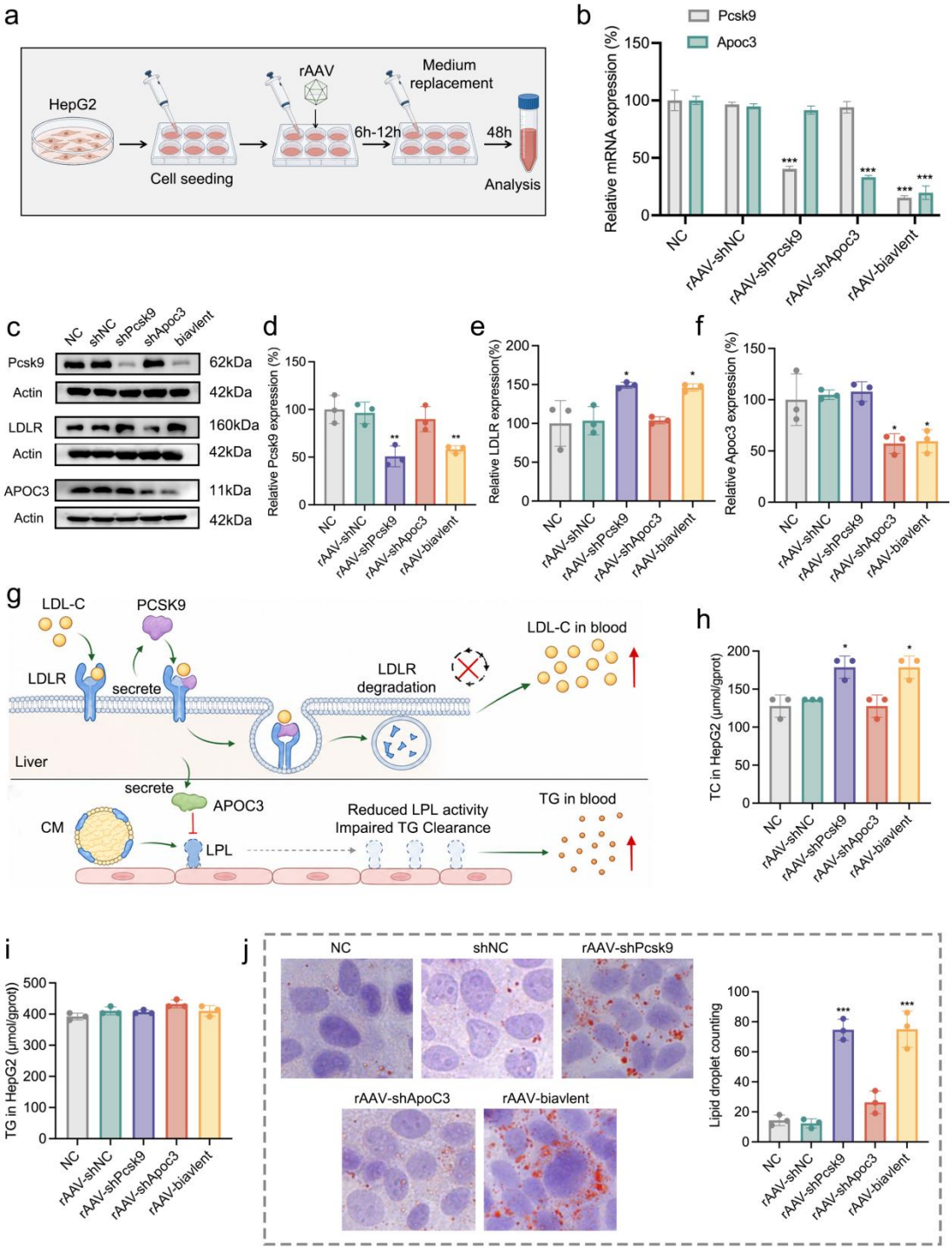


Fig.3 In Vitro Knockdown and Functional Validation of the Bivalent AAV-sh*Pcsk9*-sh*Apoc3*. **a** Schematic illustration of the in vitro experimental workflow: HepG2 cells were seeded, transfected with rAAV particles, and harvested for analysis. **b** RT-qPCR analysis of PCSK9 and APOC3 mRNA expression in HepG2 cells treated with rAAV-shPcsk9, rAAV-shApoc3 or bivalent rAAV particles in vitro. **c-f** Western blot quantification of PCSK9, LDLR and APOC3 in HepG2 cells following in vitro exposure to rAAV-shPcsk9, rAAV-shApoc3 or bivalent rAAV. **g**

Schematic illustration depicting the metabolic pathways whereby PCSK9 and APOC3 cooperatively regulate plasma LDL-C and TG homeostasis in mixed hyperlipidemia. **h** Intracellular TC levels in treated HepG2 cells. **i** Intracellular TG levels in treated HepG2 cells. **j** Representative Oil Red O staining of HepG2 cells treated with rAAV-shPcsk9, rAAV-shApoc3 or bivalent rAAV particles, with lipid droplet counting. In all relevant panels, *P < 0.05; **P < 0.01; ***P < 0.001, as determined by one-way ANOVA and two-way ANOVA.

Lipid-Lowering Efficacy of the Bivalent rAAV-sh*Pcsk9*-sh*Apoc3* in Vivo

To evaluate in vivo efficacy, 8-week-old male C57BL/6J mice were fed a high-fat diet (HFD) for 12 weeks to establish a dyslipidemia model. At week 4 of HFD feeding, mice received tail vein injections of NC, rAAV-shNC, rAAV-sh*Pcsk9*, rAAV-shApoc3, or rAAV-sh*Pcsk9*-shApoc3 (**Fig. 4a**). RT-qPCR analysis of mouse liver tissues demonstrated that rAAV-sh*Pcsk9* significantly reduced Pcsk9 mRNA levels, while rAAV-shApoc3 significantly reduced Apoc3 mRNA levels, the bivalent group achieved simultaneous knockdown of both targets with efficiency comparable to the corresponding monovalent groups (**Fig. 4b**). Western blot analysis and quantification of PCSK9, APOC3, and LDL-R protein levels in mouse liver tissues were consistent with the mRNA-level changes (**Fig. 4c-f, Fig.S7**). The bivalent vector simultaneously reduced hepatic PCSK9 and APOC3 protein levels, with knockdown efficiency comparable to that of the corresponding monovalent vectors. LDL-R expression was significantly upregulated in both the rAAV-sh*Pcsk9* and bivalent groups to a similar extent, consistent with the expected effect of PCSK9 suppression.

Serum levels of PCSK9 and APOC3 proteins in mice were also consistent with the Western blot results (**Fig. 4g and h**). Analysis of the serum lipid profile revealed distinct therapeutic effects. LDL-C levels were significantly reduced in both the rAAV-sh*Pcsk9* and bivalent vector groups (**Fig. 4i**). Consistent with this, correlation analysis revealed a significant positive correlation between PCSK9 and hepatic LDLR expression across all treatment groups (**Fig.S2**). LPL activity was significantly elevated in both the rAAV-shApoc3 knockdown group and the bivalent vector group (**Fig. 4j**), while chylomicron levels were significantly reduced (**Fig. 4k**). Correlation analysis also further revealed a significant negative correlation between APOC3 levels and LPL activity across all treatment groups (**Fig.S3**). No significant differences were observed in HDL-C levels (**Fig. 4l**). TC was significantly decreased in the Pcsk9 knockdown and bivalent groups, whereas serum TG levels were significantly reduced in the rAAV-shApoc3 and bivalent groups (**Fig. 4m–n**). The

significantly elevated LPL activity and concomitantly reduced chylomicron levels in the bivalent knockdown group further support the restoration of triglyceride clearance pathway function. Collectively, these results demonstrate that the bivalent rAAV targeting PCSK9/APOC3 achieves simultaneous regulation of both cholesterol and triglyceride metabolism, highlighting its potential for synergistic lipid-lowering therapy.

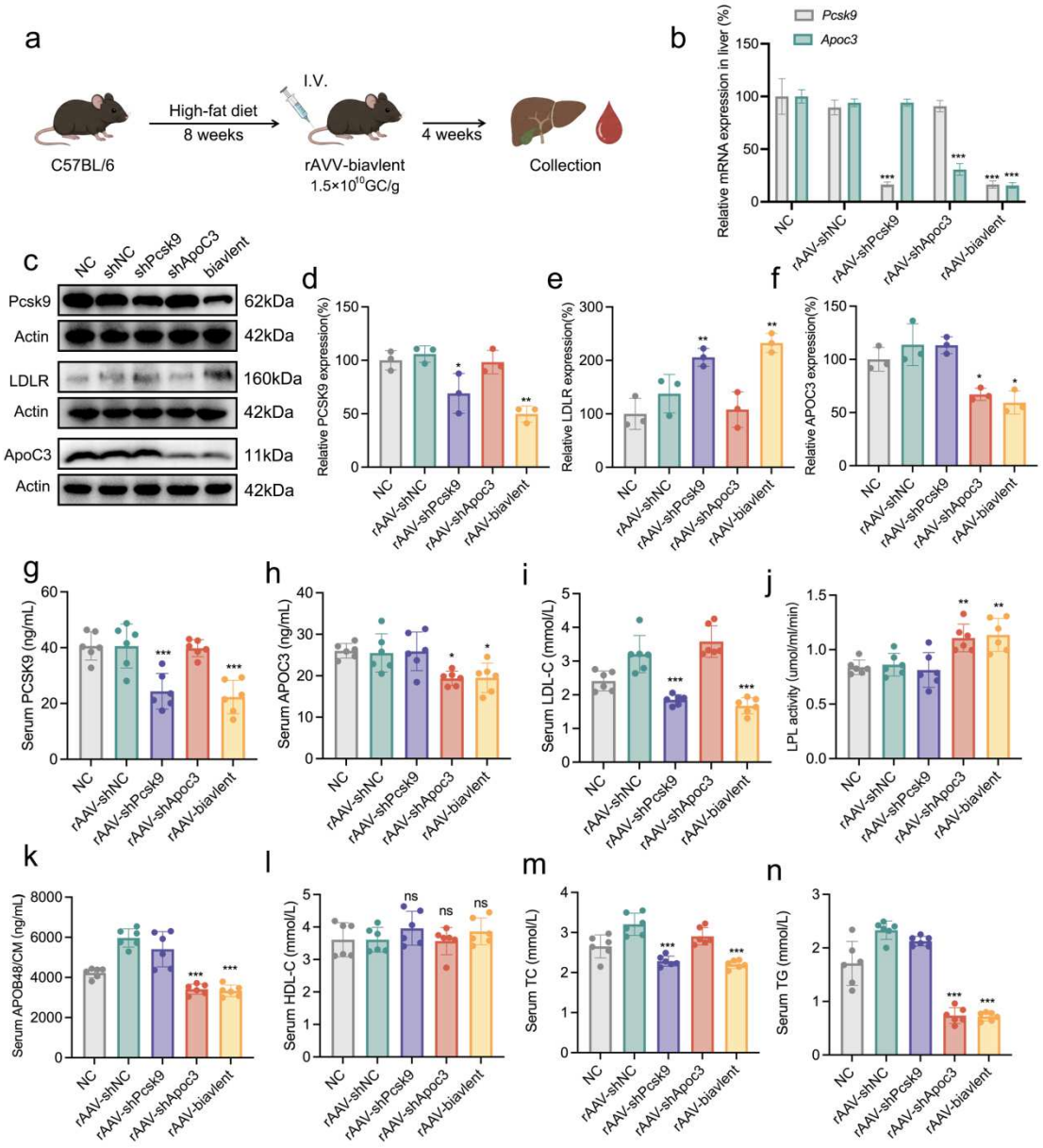


Fig.4 Lipid-Lowering Efficacy of the Bivalent rAAV-sh*Pcsk9*-sh*Apoc3* in Vivo. a Schematic overview of the in vivo experimental design. **b** RT-qPCR analysis of hepatic Pcsk9 and Apoc3 mRNA expression in mice receiving rAAV-sh*Pcsk9*, rAAV-shApoc3 or bivalent rAAV treatment. **c** Western blot analysis of hepatic APOC3 and PCSK9

protein levels in C57BL/6J mice treated with different particles. **d–f** Western blot quantification of hepatic PCSK9, LDL-R and APOC3 protein abundance in C57BL/6J mice from the above-mentioned treatment groups. **g–m** Quantification of serum PCSK9, LDL-R and APOC3 levels in C57BL/6J mice across NC, rAAV-shNC, rAAV-sh*Pcsk9*, rAAV-shApoc3 and bivalent rAAV-sh*Pcsk9*-shApoc3 groups. Data are presented as mean ± SD (n = 6 per group). *P < 0.05, **P < 0.01, ***P < 0.001 versus the NC group.

Bivalent rAAV-sh*Pcsk9*-sh*Apoc3* Alleviates Systemic Metabolic Burden in Mice

Body weight monitoring (**Fig. 5a**) showed that the NC group, maintained on a normal chow diet, exhibited the lowest body weight gain, whereas the rAAV-shNC, fed a high-fat diet (HFD), displayed the highest body weight gain, consistent with the expected HFD-induced weight gain phenotype. The body weight gain curves of the rAAV-sh*Pcsk9*, rAAV-shApoc3, and rAAV-bivalent groups were all lower than that of the rAAV-shNC group, with the rAAV-bivalent group showing relatively lower weight gain. Notably, food intake did not differ significantly among the HFD-fed groups (**Fig. S4**), indicating that the differences in body weight gain were not attributable to altered food consumption. This trend suggests that rAAV-mediated intervention targeting PCSK9/APOC3, while improving lipid metabolism, may exert a comprehensive effect on the overall metabolic status in vivo. To further substantiate this notion, metabolic cage experiments were performed to assess energy expenditure (EE) and the respiratory exchange ratio (RER) in each group. During the dark phase, when locomotor activity is highest, the EE curve of the rAAV-shNC group was higher than that of all other groups **(Fig. 5b and c)**. This phenomenon suggests that the rAAV-shNC group was under the greatest lipid burden, and the body may have required higher energy expenditure to cope with the metabolic stress imposed by the HFD. In contrast, in the PCSK9/APOC3-targeting intervention groups, the reduction in blood lipids alleviated the metabolic burden, leading to a decrease in EE that was closer to that of the NC group. The RER curves similarly showed that the rAAV-shNC group was higher than the other groups (**Fig. 5d and e**). An elevated RER generally reflects a shift in substrate utilization toward carbohydrate oxidation, which is consistent with the heavier metabolic burden and altered substrate utilization pattern in the rAAV-shNC group under HFD conditions [20]. By comparison, the RER of the monovalent and bivalent rAAV vector groups targeting PCSK9/APOC3 was closer to that of the NC group, suggesting that substrate utilization patterns tended to normalize after lipid-lowering intervention. Collectively, the rAAV-shNC group

exhibited the highest body weight gain, energy expenditure, and respiratory exchange ratio, whereas the monovalent and bivalent rAAV vector groups targeting PCSK9/APOC3 showed lower values for these metabolic parameters than the rAAV-shNC group and were closer to the NC group. These findings suggest that PCSK9/APOC3 targeting intervention may exert a comprehensive effect on the overall metabolic status in vivo by lowering blood lipids and alleviating HFD-induced metabolic burden.

Off-target Effect and In Vivo Safety Analysis

In vitro prediction based on seed sequence homology identified potential off-target genes for PCSK9 (SORCS1, TMKS, OR5B17) and for APOC3 (SMG9, TSPAN14, HKDC1). RT-qPCR validation demonstrated that the expression levels of all predicted off-target genes showed no statistically significant differences across treatment groups (**Fig. 5f-g**). These results suggest that both monovalent and bivalent constructs do not induce detectable off-target effects on the predicted candidate genes, consistent with established principles of shRNA design and off-target prediction.

Serum biochemical markers reflecting hepatic and renal function, including alanine aminotransferase (ALT), aspartate aminotransferase (AST), blood urea nitrogen (BUN), and serum creatinine (S-Cr) concentrations, remained within normal physiological ranges with no significant intergroup differences (**Fig. 5h–k**). Hematoxylin and eosin (H&E)-stained tissue sections of the heart, liver, spleen, lung, and kidney (scale bar = 100 μm) revealed no apparent pathological alterations such as congestion, hemorrhage, necrosis, or inflammatory infiltration (**Fig. 5l**). Furthermore, no significant differences were observed in the liver-to-body weight ratios among the treatment groups (**Fig. S5**), indicating that rAAV-mediated gene silencing did not induce hepatomegaly. Collectively, these data suggest that, at the dose and time frame examined in this study, the rAAV-mediated gene silencing strategy targeting PCSK9 and APOC3 exhibited an acceptable in vivo safety profile.

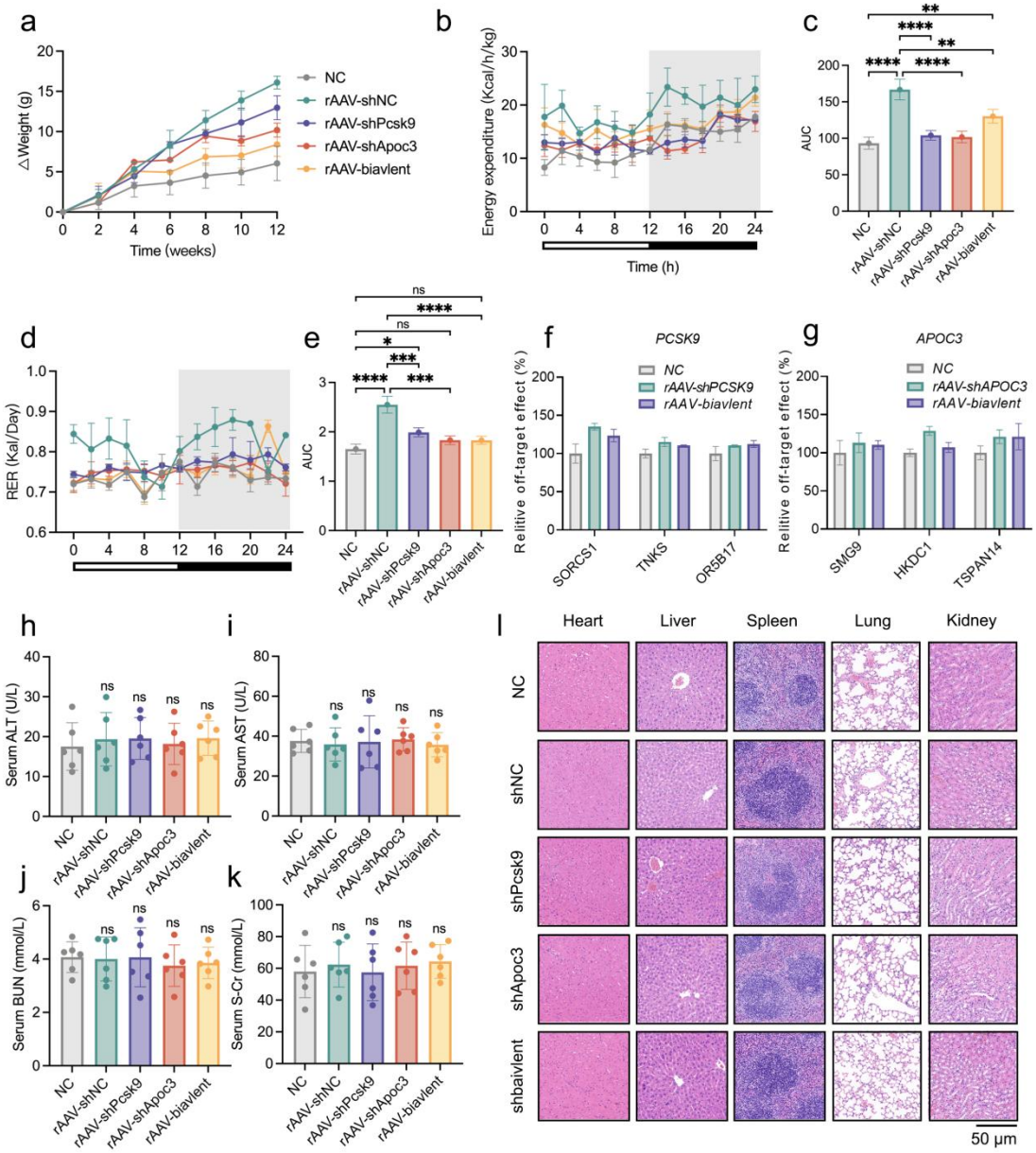


Fig. 5 Bivalent rAAV-sh*Pcsk9*-sh*Apoc3* Alleviates Systemic Metabolic Burden in Mice. Off-target Effect and In Vivo Safety Analysis. a Body-weight curves of C57BL/6J mice treated with NC, rAAV-shNC, rAAV-sh*Pcsk9*, rAAV-shApoc3 or bivalent rAAV-sh*Pcsk9*-shApoc3 particles. **b** Whole-body total energy expenditure (EE) measured by metabolic cages in C57BL/6J mice across the above-mentioned treatment groups. **c** Area under the curve (AUC) analysis for total energy expenditure traces obtained from metabolic cage recordings. **d** Respiratory exchange ratio (RER) profiles recorded using metabolic cages in each treatment group. e AUC analysis of RER curves. **f-g** In silico prediction of potential off-target genes for PCSK9 and APOC3. **h-k** Serum biochemical concentrations of ALT, AST, BUN and S-Cr in C57BL/6J mice receiving the indicated rAAV treatments. **i** Representative haematoxylin and eosin (H&E)-stained tissue sections of heart, liver, spleen, lung and kidney from

C57BL/6J mice; scale bar = 100 μm. Data are presented as mean ± SD (n = 6 per group). *P < 0.05, **P < 0.01, ***P < 0.001 versus the NC group.

DISCUSSION

In this study, we successfully established a triple-plasmid optimization strategy that effectively overcame the packaging limitations imposed by a large dual-promoter rAAV cassette. Through systematic titration of the three packaging plasmids, we found that a three-fold increase in the dose of the pHelper yielded the optimal ratio, which significantly enhanced vector yield and reduced empty capsid content. Administration of this optimized single-vector rAAV to a mouse model of mixed hyperlipidemia resulted in potent and simultaneous hepatic knockdown of PCSK9 and APOC3. These findings not only validate our initial hypothesis but also provide a potentially translatable manufacturing strategy for complex rAAV constructs, while contributing new preclinical evidence for dual target gene therapy against mixed hyperlipidemia.

Currently, the packaging of rAAV carrying large transgenic cassettes remains a major problem in the field, particularly when dual promoters are employed to achieve independent expression of two transgenes [21]. In this study, the cargo size of the PCSK9/APOC3 dual targeting construct approaches the upper packaging limit of rAAV, which inherently increases the risk of genome truncation and elevated empty capsid ratios [22]. Notably, a simple three-fold increase in the dose of pHelper effectively mitigated this risk, which can be attributed to the fact that the proteins encoded by pHelper provide essential transcriptional activation and helper functions required for rAAV genome replication and gene expression [18]. As the transgenic cassette size increases, the efficiency of AAV genome replication declines, necessitating greater auxiliary support， supplementation of pHelper dosage compensates for this deficit, ensuring sufficient helper function to support efficient replication and packaging of the oversized genome [18]. Furthermore, 1:1 balanced expression of Rep proteins, capsid proteins, and adenoviral auxiliary functions is critical for maximizing the yield of intact viral particles [23]. An overabundance of the transgene plasmid may competitively consume helper resources, whereas excessive Rep/Cap plasmid can impose cytotoxic effects due to Rep protein overexpression, both of which compromise overall productivity

[15, 23]. The optimized ratio established not only improved packaging efficiency but also reduced empty capsid ratios, addressing two key quality attributes critical for clinical translation. This optimization strategy may be broadly applicable to other large-cargo or structurally complex rAAV constructs [24].

Having established the optimized three-plasmid ratio, we obtained high-quality viral stocks and subsequently validated their therapeutic efficacy in a mouse model of mixed hyperlipidemia. The results demonstrated that this optimized single-vector rAAV produced efficient hepatic silencing of both PCSK9 and APOC3, accompanied by robust lipid-lowering effects, with serum TC and TG reduced by approximately 30% and 70%. This “single rAAV co-targeting” strategy is of particular significance for mixed hyperlipidemia and ASCVD [21]. Furthermore, the single-vector design ensures co-delivery of both targeting sequences to the same hepatocyte, representing a key advantage over administration of two separate rAAV vectors [25, 26]. Compared to the unoptimized system, the approximately 40% improvement in transfection efficiency further underscores the translational potential of this optimized platform. Notably, histological examination of major organs revealed no overt tissue damage, and liver function parameters remained within normal ranges, indicating that this straightforward strategy offers favorable tolerability at the therapeutic dose, and the enhanced editing efficiency, lower manufacturing costs, and improved safety profiles in clinical settings.

Based on this study, we will further validate the long term safety and efficacy of this platform in animal models that more closely recapitulate the clinical setting, and to advance the manufacturing process toward pilot production. Concurrently, we will also explore the applicability of this optimization strategy to other large cargo or multi-target rAAV constructs, with the aim of providing a more broadly applicable solution for the efficient production of gene therapy vectors.

ACKNOWLEDGEMENTS

This work was supported by the Technological Innovation and Application Development Program of Chongqing (CSTB2023TIAD-STX0009), China Postdoctoral Science Foundation General Program (2026M793961), China Postdoctoral Science Foundation Special Support (2026T190643), National Natural Science Foundation of China (82607381), Chongqing Special Project for Out-

standing Graduate Student Cultivation Program of Chongqing Medical University (No. BJRC202321).

AUTHOR CONTRIBUTIONS

J. H. was responsible for data collection, analysis, and drafting of the manuscript. Y.Y.H. contributed to data collection and interpretation. Y.F.Z. provided advice on experimental design, contributed to data analysis and interpretation, co-wrote the manuscript, and secured funding support. G.Z., M.J.D., L.M.Y., and K.H. provided advice on the animal experimental design. Y.X.C. and C.Y. supervised and administered the project and secured funding support. All authors reviewed and approved the manuscript.

COMPETING INTERESTS

The authors declare no conflict of interest.

REFERENCES

1. Berberich AJ, Hegele RA. A Modern Approach to Dyslipidemia. Endocr Rev. 2021;43:611-53.

2. Brouwers MCGJ, Greevenbroek MMJV, Stehouwer CDA, Graaf JD, Stalenhoef AFH. The genetics of familial combined hyperlipidaemia. Nat Rev Endocrinol. 2012;8:352-62.

3. Ginsberg HN, Packard CJ, John CM, Jan B, Aguilar-Salinas CA, Maurizio A et al. Triglyceride-rich lipoproteins and their remnants: metabolic insights, role in atherosclerotic cardiovascular disease, and emerging therapeutic strategies—a consensus statement from the European Atherosclerosis Society. Eur Heart J.2021;42:4791-806.

4. Borén J, Chapman MJ, Krauss RM, Packard CJ, Bentzon JF, Binder CJ et al. Low-density lipoproteins cause atherosclerotic cardiovascular disease: pathophysiological, genetic, and therapeutic insights: a consensus statement from the European Atherosclerosis Society Consensus Panel. Eur Heart J. 2020;41:2313-30.

5. Girón GO, Otero S, Nikolaou PE, Alcover S, Ramos-Regalado L, Zaragoza C et al. Atherogenic dyslipidaemia and residual cardiovascular risk: Understanding the link to heart disease. European Journal of Clinical Investigation 2026; 56:e70167.

6. Guan Y, Liu X, Yang Z, Zhu X, Liu M, Du M et al. PCSK9 Promotes LDLR Degradation by Preventing SNX17-Mediated LDLR Recycling. Circulation 2025; 151: 1512-26.

7. Packard CJ, Pirillo A, Tsimikas S, Ference BA, Catapano AL. Exploring apolipoprotein C-III: pathophysiological and pharmacological relevance. Cardiovasc Res. 2023;119:2843-57.

8. Ballantyne CM, Norata GD. The evolving landscape of targets for lipid lowering: from molecular mechanisms to translational implications. Eur Heart J.2025; 46:4737-50.

9. Sethi Y, Mahajan K, Shapiro MD, Banach M. Beyond therapeutic maximalism: Prioritization and personalization in preventive therapies. Prog Cardiovasc Dis.2026; 96:4-7.

10. Belgrad J, Tang Q, Hildebrand S, Summers A, Sapp E, Echeverria D et al. A programmable dual-targeting di-valent siRNA scaffold supports potent multi-gene modulation in the central nervous system. Nucleic Acids Res.2023; 52:6099-113.

11. Han Z, Tan C, Ai J, Zhu Y. In vivo adeno-associated virus-mediated LDLR/PCSK9 intervention for familial hypercholesterolemia. Genes Dis. 2025;12:101632.

12. Zheng Q, Zhang X, Yang H, Xie J, Zhong C. Internal Ribosome Entry Site Dramatically Reduces Transgene Expression in Hematopoietic Cells in a Position-Dependent Manner. Viruses. 2019:11:920.

13. Lin J, Lin Y, Liu N, Cao W, Zhang J, Wen S et al. AAVLINK: A potent DNA-recombination method for large cargo delivery in gene therapy. Cell.2026; 189: 969–86.

14. Pistek M, Andorfer P, Grabherr R, Kraus B, Hernandez Bort JA. Factors affecting rAAV titers during triple-plasmid transient transfection in HEK-293 cells. Biotechnol Lett. 2024;46:945-59.

15. Park S, Shin S, Lee H, Jang JH, Lee GM. Enhancing the production of adeno‐associated virus (AAV)2 and AAV9 with high full capsid ratio in HEK293 cells through design‐of‐experiment optimization of triple plasmid ratio. Biotechnol J. 2024;19:e2300667.

16. Nguyen TNT, Sha S, Hong MS, Maloney AJ, Barone PW, Neufeld C et al. Mechanistic model for production of recombinant adeno-associated virus via triple transfection of HEK293 cells - ScienceDirect. Mol Ther Methods Clin Dev. 2021;21:642-55.

17. Sofia F, Joana D, Ana Sofia C. Mammalian Stable Cell Platforms for Recombinant Adeno-associated Virus (rAAV) Production: Development Strategies and their Impact on Viral Productivity. Curr Gene Ther. 2023;23:184-97.

18. Van Lieshout L, Costa-Grant K, Lata D, Zacarias A, Ota S, Adusei A et al. An engineered helper plasmid generates differential E4orf6 and L4-22/33K gene expression increasing AAV vector production. Gene Ther. 2026;33:505-14.

19. Brummelkamp, T. R. A System for Stable Expression of Short Interfering RNAs in Mammalian Cells. Science. 2002;296:550-53.

20. Hansen M, Lange KK, Stausholm MB, Dela F. Are Individuals With Type 2 Diabetes Metabolically Inflexible? A Systematic Review and Meta‐Analysis. Endocrinol Diabetes Metab. 2025;8:e70044.

21. Kolesnik VV, Nurtdinov RF, Oloruntimehin ES, Karabelsky AV, Malogolovkin AS. Optimization strategies and advances in the research and development of AAV-based gene therapy to deliver large transgenes. Clin Transl Med. 2024;14:e1607.

22. Blahetek G, Lindner B, Oti M, Schn C, Strobel B. AAV yield, bioactivity, and particle heterogeneity are impacted by genome size and non-coding DNA elements. Mol Ther Methods Clin Dev. 2025;33:101499.

23. Catalán-Tatjer D, Tzimou K, Nielsen LK, Lavado-García J. Unravelling the essential elements for recombinant adeno-associated virus (rAAV) production in animal cell-based platforms. Biotechnol Adv. 2024;73:108370.

24. Tzimou K, Hulsbus-Andreu P, Yildirim EB, Nielsen LK, Lavado-García J. Mixture design as a tool for improving full-to-empty particle ratios across various GOIs in rAAV production. Gene Ther. 2026;33:48-56.

25. Maestro S, Weber ND, Zabaleta N, Aldabe R, Gonzalez-Aseguinolaza G. Novel vectors and approaches for gene therapy in liver diseases. JHEP. 2021;3:100300.

26. Ledri M, Kokaia M. Gene therapy for epilepsy: An emerging, promising approach for a serious neurological disorder. J Intern Med. 2026;299:302-327.

Supplementary Files

This is a list of supplementary files associated with this preprint. Click to download.

- Supportinginformation.docx